J. Chem. Chem. Eng. 13 (2019) 23-33
doi: 10.17265/1934-7375/2019.01.003

Computational Design of Azo-anthraquinone Schiff Base Mn Complexes as Mediators for Biofuel Cell Cathode

Kazuto Kajiwara[1], Shinsuke Yamane[1], Tomoyuki Haraguchi[1], Sayantan Pradhan[2], Chittaranjan Sinha[3], Rakesh Parida[4], Santanab Giri[4], Gourisankar Roymahaptra[5], Dohyun Moon[6] and Takashiro Akitsu[1]

1. Department of Chemistry, Faculty of Science, Tokyo University of Science, Tokyo, Japan

2. Chemical Sciences Division, Saha Institute of Nuclear Physics, Kolkata, West Bengal, India

3. Department of Chemistry, Jadavpur University, Kolkata, West Bengal, India

4. Department of Chemistry, National Institute of Technology, Rourkela, India

5. Department of Applied Sciences, Haldia Institute of Technology, Haldia, West Bengal, India

6. Beamline Department, Pohang Accelerator Laboratory, Pohang, Korea

Abstract: The cathode of biofuel cell reduces molecular oxygen to water using four electrons, an enzyme of multicopper oxidase family, laccase, is contained, though its electron transfer efficiency from the electrode resulted in rate determining process. To improve this electron, transfer via mediators, we have investigated several mediator metal complexes between the electrode and laccase, in particular hydrophobic pocket on the surface. We have discussed DFT computational results and selected experimental data of new Mn(III/II) Schiff base complexes having redox active (anthraquinone) ligands and photochromic (azobenzene) ligands about azobenzene moiety at the sole molecular level. Moreover, we carried out computational docking simulation of laccase and complexes considering *trans-cis* photoisomerization (electronic states) and Weigert effect (molecular orientation to fit better) of azobenzene moiety. Additionally, actual experimental data also presented to indicate the expected merits for mediators.

Key words: Laccase, Schiff base, Mn complex, anthraquinone, azobenzne, computational chemistry.

1. Introduction

(Bio) fuel cells are promising renewable power source for the sustainable development of the environment with reference in particular to green chemistry and technology [1]. Laccase, a multicopper oxidase (MCO) enzyme, reduces oxygen to water and has been used as enzyme on the cathode side of enzyme type biofuel cell [2-4]. Rate of cathodic reduction depends on the efficiency of long-range electron transfer process. To improve this electron transfer, we have investigated several types of metal complexes as mediators between the electrode and laccase [5-11]. Molecular docking of suitable compound (both ligands and complexes) to the hydrophobic pocket of laccase may be useful in predicting the redox activity and their utility in biofuel cells [8, 9]. Presence of noncoordinating, non-innocent substituent to the ligand backbone in the metal ligand or complex may be induced by the polarized UV-light to control the rate of redox processes. In particular, the pendant azobenzene moiety can show Weigert effect (molecular alignment induced by polarized UV light) to control molecular orientation for suitable fitting [10, 11].

Herein, we present rationally molecular design of new Mn(III/II) Schiff base (H_2L^1 = 2-hydroxy-3-methoxy-5-phenyldiazobenzaldehydene-1,2-diaminoanthraquino ne (1), H_2L^2 = 2-hydroxy-5-phenyldiazobenzaldehydene-1,2-diamino anthraquinone (2), H_2L^3 = 2-hydroxy-3-methoxy-5-phenyldiazobenzaldehydene-2,3-diaminoanthraquinone (3)) complexes where a tetradentate dianionic N_2O_2 core is obtained by the

Corresponding author: Takashiro Akitsu, Ph.D., professor, research field: inorganic coordination chemistry.

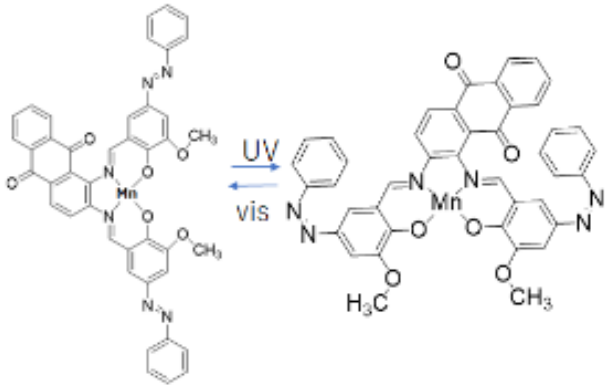

Scheme 1 ***Trans*** **(left) –** ***cis*** **(right) photoisomerization of 1.**

condensation of 1,2-diaminoanthraquinone and 2-hydroxy-3-methoxy-5-phenyldiazobenzaldehyde, 1,2-diaminoanthraquinone and 2-hydroxy-5-phenyldiazobenzaldehyde, or 2,3-diaminoanthraquinone 2-hydroxy-3-methoxy-5-phenyldiazobenzaldehyde, respectively. The Schiff bases bear a redox active (anthraquinone) moiety and photochromic (azobenzene) moiety [11]. Actually only the best complex expected (1) (Scheme 1) are characterized structurally. Both electrochemical and photochromic properties are examined and have been compared with the DFT/TD-DFT computed functions and computational docking simulation to laccase which were carried out prior to actual experiments.

2. Materials and Methods

2.1 General Procedure

Chemicals and solvents were of commercial grade obtained from SIGMA-ALDRICH, Tokyo Chemical Industry, and Wako, especially metal salts from SIGMA-ALDRICH. These were used as received without further purification.

2.2 Physical Measurements

Infrared (IR) spectra were recorded as KBr pellets on a JASCO FT-IR 4200 plus spectrophotometer in the range 4,000–400 cm^{-1} at 298 K. UV-vis spectra were obtained on a JASCO V-570 UV-vis-NIR spectrophotometer in the range 1,500–200 nm at 298 K. Electrochemical (cyclic voltammetry, CV) were carried out on a BAS SEC2000-UV/VIS and ALS2323 system with Ag/AgCl electrodes range of -0.50–0.80 V vs. Ag/Ag^{+}.

2.3 Preparations

2-Hydroxy-3-methoxy-5-phenyldiazobenzaldehyde, and 2-hydroxy-5-phenyldiazobenzaldehyde (as precursors of H_2L^1 and H_2L^2) were prepared according to the literature procedure using the corresponding precursor aldehydes [11]. Each of them (0.06 g, 0.25 mmol) was added to a methanol solution (80 mL) of 1,2-diaminoanthraquinone (SIGMA-ALDRICH) (0.13 g, 0.5 mmol) to stir for 2 hr at 318 K, then $Mn(CH_3COO)_2 \cdot 4H_2O$ (SIGMA-ALDRICH) (0.061 g, 0.025 mmol) was added to stir for 2 hr at 318 K. Brown crude product was obtained by filtration after evaporation and the product was recrystallized from hexane and dried to give rise to 1 or 2.

1: Yield 18.0 %. IR (KBr, cm^{-1}) 715(m), 838(w), 1019(w), 1127(w), 1164(w), 1193(w), 1303(s), 1328(m), 1382(m), 1439(m), 1531(s), 1588(m), 1625(m), 3268(m), 3414(s).

2: Yield 12.7 %. IR (KBr, cm^{-1}) 715(m), 838(w), 1019(w), 1164(w), 1193(w), 1303(s), 1329(m), 1380(m), 1441(m), 1531(s), 1588(m), 1624(m), 3270(m), 3414(s).

2.4 X-ray Crystallography

Powder X-ray diffraction patterns of 1 were collected at 298 K at Pohang Light Source II 2D Supramolecular Crystallography Beamline (PLSII-2D-SMC). Powder was packed in the 0.5 mm diameter (wall thickness is 0.01 mm) capillary and the diffraction data measured transparency as Debye-Scherrer at 298 K respectively, with the 100 mm of detector distance in 10 sec exposures with synchrotron radiation (λ = 1.20007 Å) on an ADSC Quantum-210 detector at 2D SMC with a silicon (111) double crystal monochromator (DCM) at the Pohang Accelerator Laboratory, Korea. The PAL BL2D-SMDC

Table 1 Crystallographic data for 1.

	1
Empirical formula	C42H28MnN6O6
Formula weight	767.64
Temperature / K	298
Crystal system	Triclinic
Space group	P-1
a/Å	17.20(2)
b/Å	26.21(3)
c/Å	11.670(15)
α / °	97.38(8)
β / °	94.90(6)
γ / °	104.67(7)
V/(Å^3)	5418(27)
Z	2
D/gcm^{-3}	0.430
F(000)	726
S	11.2135
Rwp(%)	14.73

program [12] was used for data collection, and Fit2D program [13] was used converted 2D to 1D pattern and wavelength and detector distance refinement. Rietveld analysis20 was carried out with a Rigaku PDXL2 ver.2.2.1.0, commercially available program package by the following procedures: indexing, cell and space group determination, input composition and initial structural model from DFT, direct space method, addition of displacement parameters for non-hydrogen atoms, and refinement with hydrogen atoms under restraint. Crystallographic data are listed in Table 1.

2.5 Computational Methods

Calculations of all complexes were performed using the Gaussian 09W software Revision D.02 (Gaussian, Inc.) [14]. All the geometries have been optimized by using B3LYP level of theory and SDD as basis set. Also, we performed frequency calculation on optimized geometry by using same level of theory and basis set also.

Docking of metal complexes has been performed out with AutoDock 4.2.6 on windows platform with 8 GB RAM and Intel I 5 processor [15].

3. Results and Discussion

3.1 Synthesis and Formulation

As mentioned in later sections about computational results, only 1 and 2 were prepared actually. In IR spectra, characteristic C=N bands of imine groups coordinating to Mn(II) ion appeared at 1,625 and 1,624 cm^{-1} for 1 and 2, respectively. Which are similar to analogous Mn(II) complexes [16], and this feature exhibits high-wavenumber shift comparing to common Schiff base Mn(III) complexes (1,616 cm^{-1}, [17]). Hence air oxidation of Mn(II) as prepared to Mn(III) immediately [18] during reaction did not occur. Selected possible assignments of other bands for example 1 are as follows: 715(δCH), 1127(C-O), 1303(C-N), 1439(Ar), 1588(Ar), 1625(C=O), and 3414 cm^{-1} (O-H).

UV-vis spectra appeared intense π–π* and n–π* peaks and moderate d-d peaks at 270, 345, and 540 nm for 1 and 275, 345, and 545 nm for 2, which were typical features of a square planar Schiff base Mn(II) complex with azo-ligand in a ground spin state [10]. Introduction of methoxy group makes them blue shifts. For 1, *trans* to *cis* photoisomerization after UV light irradiation (and also reverse changes by visible light) attributed to spectral changes, namely slight decrease of intensity around 270 nm of π–π* band, significant decrease of intensity around 345 nm of n– π*, and drastic blue shift 550 to 450 nm of d-d band. However, 2 did not exhibit smooth photoisomerization.

Complex 1 affords a four-coordinated slightly distorted square planar *trans*-[N_2O_2] coordination geometry. Fig. 1 shows the crystal structure of 1 with Mn1-O1 = 1.771(3), Mn1-O4 = 1.781(2), Mn1-N1 = 1.903(3), Mn1-N4 = 1.883(2) Å, O1-Mn1-N1 = 171.405(16), O4-Mn1-N4 = 172.763(13) °). Within the precision of powder analysis, ligand moiety (such as N2-N3 = 1.2304(15) Å, N5-N6 = 1.2474(17) Å) exhibited normal values of geometry, which was similar to DFT optimized structure (see next section). Of course, not only in solutions (but also in crystals),

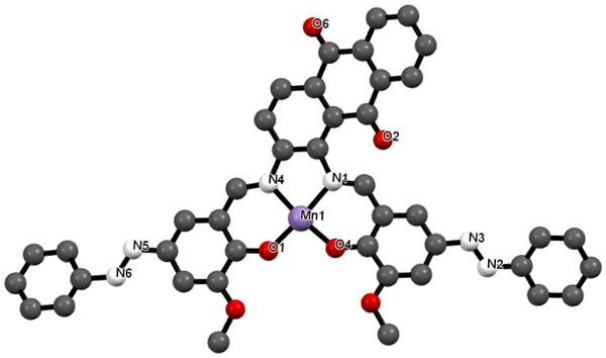

Fig. 1 Crystal structure of 1 analyzed from powder diffraction data.

empty apical sites accept axial ligands such as water or solvents molecules potentially [10].

3.2 Selection of Ligands

By using TD-DFT, candidate molecules were examined prior to actual experiments. Figs. 2-4 depict optimized structures of *trans*-form of 1-3 assuming as sextet states, respectively. Total energies were -2,500.674, -2,271.662, and -2,271.675 a.u., respectively. HOMO and LUMO energies were as follows: alpha HOMO = -0.377, -0.392, -0.402 a.u. beta HOMO = -0.366, -0.370, -0.372 a.u. alpha LUMO = -0.301, -0.305, -0.303 a.u. LUMO = -0.357, -0.362, -0.364 a.u. for *trans*-forms of 1-3, respectively. Calculated UV-vis spectra appeared intense peaks at 549.429, 525.534, and 535.060 nm, respectively. In this way, methoxy group more importantly contributed to spectral shift than anthraquinone moiety of the ligand, and comparison between 1 and 2 may be useful for molecular design reasonably. Additionally, PDOS with orbital contribution and UV-vis spectra and possible transitions in 1-3 (and their Cu(II) analogues for comparison) were also shown in Supplementary Information 1 and 2.

3.3 Cis-trans Photoisomerization of Ligands

Assuming photoisomerization of azobenzene moiety vertially, *trans*-forms (see section 3.2) and *cis*-forms were compared not only for 1-2 but also their Cu(II) analogues. According to DFT results, all complexes could be expected to exhibit *cis-trans*

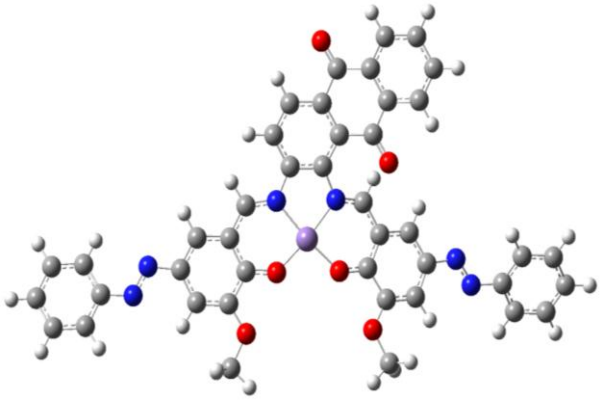

Fig. 2 Optimized structure of 1.

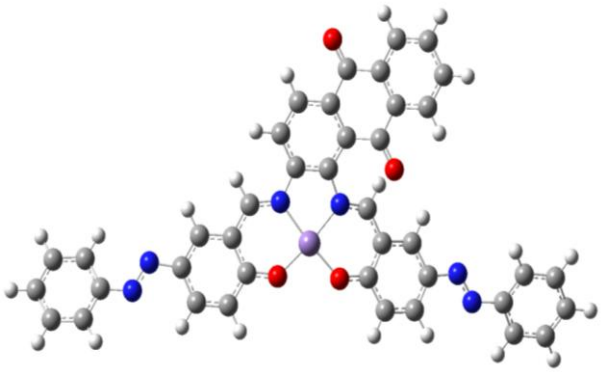

Fig. 3 Optimized structure of 2.

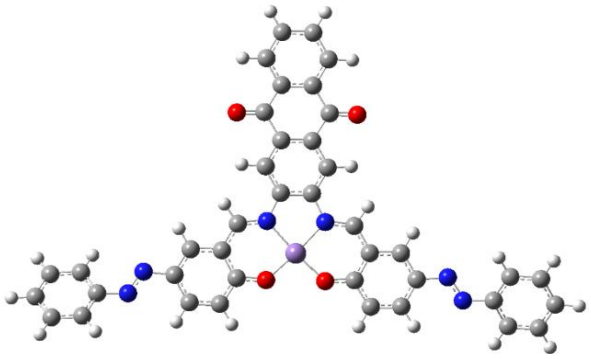

Fig. 4 Optimized structure of 3.

photoisomerization with significant changes. Large shifts of optical absorption associated with redox potentials of *cis*-form of 1 indicated that it may be the most appropriate complexes among them for the purpose as mediators. Total energies were -2,500.672 and -2,271.615 a.u., respectively. HOMO and LUMO energies were as follows: alpha HOMO = -0.355 and -0.384 a.u. beta HOMO = -0.352 and -0.357 a.u. alpha LUMO = -0.324 and -0.339 a.u. LUMO = -0.339 and -0.350 a.u. for *cis*-form of 1 and 2, respectively.

Calculated UV-vis spectra appeared intense peaks at 836.26 and 605.598 nm, respectively. Additionally, PDOS with orbital contribution and UV-vis spectra and possible transitions in 1 and 2 were also exhibited in Supplementary Information 3 and 4.

3.4 Docking of Complexes into Laccase

By using simulation, docking ability to laccase for 1-3 was investigated as follows. The A chain of laccase is modified by removing water and bound ligand. Missing amino acids have been checked and hydrogen bonds have been added to the protein structure. Center Grid box x:16.895, y:5.931, z:37.151 and number of points in x, y, z dimensions are considered as 30×30×30 $Å^3$ respectively and grid spacing has been taken as 0.3750 Å. The protein (Laccase) and ligand (complexes) structures have been modified by Autodock Tools. Ligands have been prepared by adding Gasteiger charges, detecting root and choosing torsions from torsion tree of Autodock Tools panel [19]. Docking procedure has been performed by using Lamarckian genetic algorithm [20]. The best-fit ligand conformations were selected based on their minimum binding energies.

Docking scores of complexes (DFT optimized structures) to crystal structure of laccase (retrieved from PDB 1qyc) were -9.6, -8.3, and -7.9 kcal/mol for *trans*-forms of 1-3, respectively. On the other hand, docking scores of the corresponding Cu complexes were -9.7, -9.2, and -8.7 kcal/mol for *trans*-forms of 1-3's Cu(II) analogues, respectively. The results indicated that docking scores mainly depend on structures of ligands, and ligand 1 was the best fit ligand among three as *trans* form.

3.5 Docking of cis Form Assuming Polarized UV Light Irradiation.

Importance of *trans-cis* isomerization of azo-group (by UV natural light irradiation), orientation change (by UV polarized light irradiation, so-called Weigert effect [10, 11]), or both was simulated by comparison of *trans- and cis-* forms of 1 to fit laccase surface. Indeed, the docking scores were -9.6 and -9.6 kcal/mol, because steric factor due to photoisomerization was not conclusive in this case. Unfortunately, molecular orientation by Weigert effect was not clear based on the results. However, electronic factors calculated also proved that *cis-form* of 1 was the best fit mediator, though not only *trans-* (Fig. 5) but also *cis*-form (Fig. 6) of 1 can similarly fit to laccase according to simulation. Secondary structure of laccase receptor represented by ribbon model, and *cis*-form of 1 is represented by ball and stick model.

A table of Supplementary Information 5 listed detailed data of docking of *cis*-form of 1 through hydrophobic, electrostatic, and hydrogen bonding interactions. Comprehensive perception of laccase receptor and *cis*-form of 1 interaction after docking. The *cis*-form of 1 is docked near T1 active site of laccase receptor on surface.

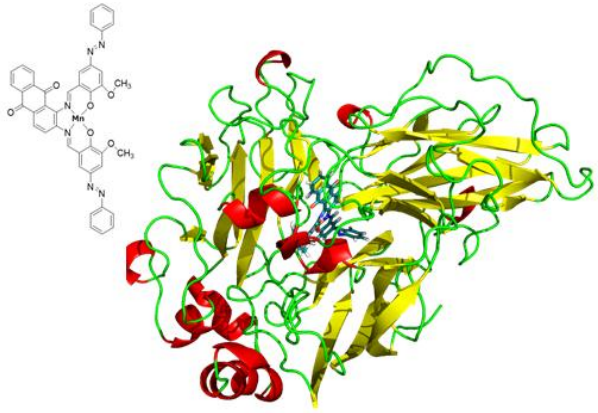

Fig. 5 Docking simulation of *trans*-form of 1 and laccase.

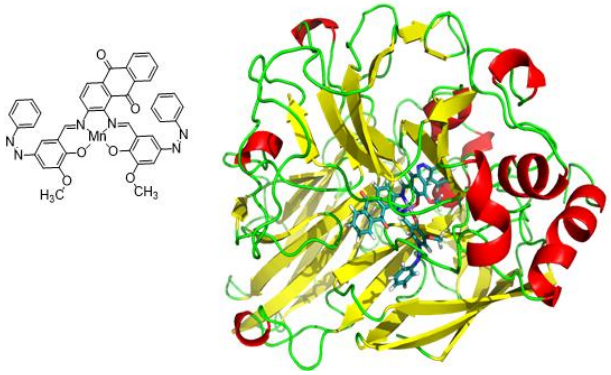

Fig. 6 Docking simulation of *cis*-form of 1 and laccase.

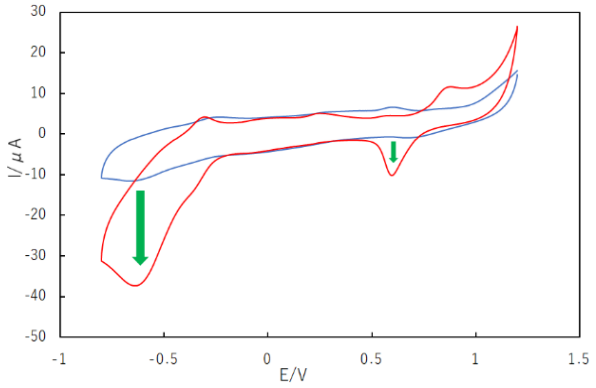

Fig. 7 CV (as glassy carbon electrode) of laccase containing (*trans-*)1 under nitrogen (blue) and oxygen (red) atmosphere.

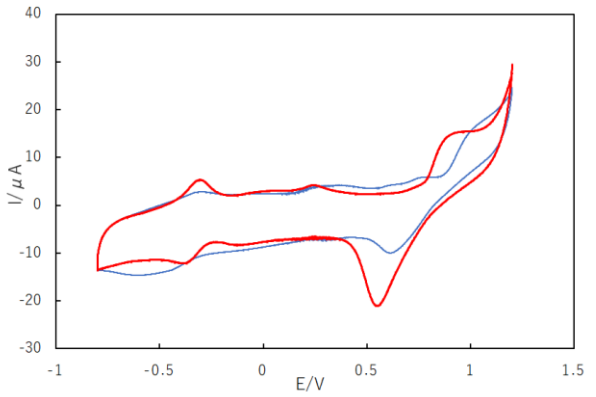

Fig. 8 CV (measured with grassy carbon) 1 after photoisomerization. Red: UV 0 min (*trans*), Green: UV 5 min (*cis*), Blue: UV 10 min (*cis*).

3.6 Electrochemistry

Changes of UV-vis spectra (in DMSO solution), decreasing n–π* band intensity around 450 nm after UV light irradiation, shown in in Supplementary Information 6 suggested that the azo-ligand complex solely exhibited smooth photoisomerization in a solution.

Fig. 7 shows CV (as glassy carbon electrode) of laccase containing (trans-form of) 1 under nitrogen and oxygen purged atmosphere. Increasing current under oxygen atmosphere suggested that reduction of oxygen occurred effectively by 1 [10, 11]. However, both are measured as *trans*-forms, because photoisomerization could not be observed in laccase's hydrophobic pocket for this complex, contrary to glassy carbon environment (Fig. 8). Supramolecular hybrids of laccase and metal complex, especially actual features of unsuitable molecular recognition, made impossible to use not only photoisomerization but also photo-induced orientation of azo-ligand.

4. Conclusions

In this way, a computationally-driven style in screening of suitable complexes was carried out, contrary to a conventional style, namely preparations, characterizations, and computational consideration. The only best complex 1 with laccase was examined experimentally to proof an assumption of molecular design by screening.

<Computational tests>

- DFT of complex molecules (1, 2, 3) in Section 3.2
- DFT of *cis-trans* photoisomerization (1, 2) in Section 3.3
- Docking of a complex into laccase (1) in Section 3.4

<Experimental tests>

- Characterization (1, partly 2) in Section 3.1
- Electrochemistry (1) in Section 3.6

As expected by computation of three candidates, we have experimentally measured changes UV-vis and CV of 1 solely showing *cis*-trans photoisomerization of azo-group smoothly. Purged gas CV exhibited effective oxygen reduction by laccase with mediator of 1 was confirmed because of spatial advantage. However, *trans-cis* photoisomerization and/or Weigert effect of azobenzene moiety were not observed clearly for 1 as docking to laccase due to unsuitable molecular recognition actually.

Supplementary data

PDOS with Orbital Contribution, UV-*vis* spectra and possible transitions, details of docking and UV-*vis* (DMSO) by photoisomerization are provided.

Acknowledgment

The synchrotron X-ray crystallography experiment

at PLS-II BL2D-SMC beamline was supported in part by MSIT and POSTECH. The laboratory XRD work was partly conducted at the Advanced Characterization Nanotechnology Platform of the University of Tokyo (Prof. Kazuhiro Fukawa), supported by the Nanotechnology Platform of the Ministry of Education, Culture, Sports, Science and Technology (MEXT), Japan.

References

[1] Mano, N., and de Poulpiquet, A. 2018. "O_2 Reduction in Enzymatic Biofuel Cells." *Chem. Rev.* 118: 2392 and references therein.

[2] Agbo, P., Heath, J. R., and Gray, H. B. 2014. "Modeling Dioxygen Reduction at Multicopper Oxidase Cathodes." *J. Am. Chem. Soc.* 136: 13882.

[3] Winkler, J. R., and Gray, H. B. 2014. "Long-Range Electron Tunneling." *J. Am. Chem. Soc.* 136: 2930.

[4] Crane, B. R., Di Billio, A. J., Winkler, J. R., and Gray, H. B. 2001. "Electron Tunneling in Single Crystals of Pseudomonas Aeruginosa Azurins." *J. Am. Chem. Soc.* 123: 11623.

[5] Kurosawa, Y., Tsuda, E., Takase, M., Yoshida, N., Takeuchi, Y., Mitsumoto, Y., and Akitsu, T. 2015. *Threonine: Food Sources, Functions and Health Benefits.* NY, USA: Nova Science Publishers.

[6] Ogikubo, Y., Sano, A., Nagano, K., and Akitsu, T. 2016. *Laccase: Applications, Investigations and Insights.* NY, USA: Nova Science Publishers.

[7] Ogikubo, Y., and Akitsu, T. 2016. "Enhancing Medical or Biological Functions of Laccase by Cyanide-Bridged Cu(II)-Fe(III) Bimetallic Complexes Madiators." *Drug Designing: Open Access* 5: 130.

[8] Takeuchi, Y., and Akitsu, T. 2016. "Anthraquinone Derivative Chiral Schiff Base Copper(II) Complexes for Enzyme Type Bio-Fuel Cell Mediators." *J. Elect. Eng.* 4: 189.

[9] Takeuchi, Y., Sunaga, N., and Akitsu, T. 2017. "Anthraquinone and L-amino Acid Derivatives Schiff Base Cu(II) Complexes as a Mediator between Cathode of Biofuel Cell and Oxygen-reducing Laccase." *Trends in Green Chem.* 3: 1.

[10] Mitsumoto, Y., Sunaga, N., and Akitsu, T. 2017. "Polarized Light Induced Molecular Orientation in Laccase for Chiral azo-salen Mn(II), Co(II), Ni(II), Cu(II), Zn(II) Mediators toward Application for Biofuel Cell." *Sci. Fed. J. Chem. Res.* 1: 1.

[11] Sano, A., Yagi, S., Haraguchi, T., and Akitsu, T. 2018. "Synthesis of MnII and CuII Complexes Including a Zobenzene and Its Application to Mediators of Laccase for Biofuel Cells." *J. Indian. Chem. Soc.* 95: 487.

[12] Shin, J. W., Eom, K., and Moon, D. 2016. "BL2D-SMC, the Supramolecular Crystallography Beamline at the Pohang Light Source II, Korea." *J. Synchrotron Rad.* 23: 369.

[13] Fit2D program: Andy Hammersley (E-mail: hammersley@esrf.fr), ESRF; 6 RUE JULES HOROWITZ BP 220 38043 GRENOBLE CEDEX 9 FRANCE.

[14] Frisch, M. J., Trucks, G. W., Schlegel, H. B., Scuseria, G. E., Robb, M. A., Cheeseman, J. R., Scalmani, G., Barone, V. et al. 2009. Gaussian 09, Revision D.01, Gaussian, Inc., Wallingford CT, 2009.

[15] Morris, G. M., Huey, R., Lindstrom, W., Sanner, M. F., Belew, K. R., Goodsell, D. S., and Olson, A. J. 2009. "AutoDock4 and AutoDockTools4: Automated Docking with Selective Receptor Flexibility." *J. Comput. Chem.* 30: 2785.

[16] Akitsu, T., and Tanaka, R. 2011. "Polarized Spectroscopy and Polarized UV Light-induced Molecular Orientation of Chiral Diphenyl Schiff Base Ni(II) and Cu(II) Complexes and Azobenzene in a PMMA Film." *Current Phys. Chem.* 1: 82.

[17] Akitsu, T., Takeuchi, Y., and Einaga, Y. 2005. "Diaqua(N,N'-bis(3,5-dibromosalicylidene)(*1R,2R*)-1,2-diaminocyclohexanato-κ^4O,N,N',O')manganese(III)) Perchlorate Dehydrate." *Acta Cryst.* E61: m772.

[18] Okamoto, Y., Nidaira, K., and Akitsu, T. 2012. *Crystallography: Research, Technology and Applications*. NY, USA: Nova Science Publishers, Inc.

[19] Gasteiger, J., and Marsili, M. 1980. "Iterative Partial Equalization of Orbital Electronegativity—A Rapid Access to Atomic Charges." *Tetrahedron.* 36: 3219.

[20] Morris, G. M., Goodsell, D. S., Halliday, R. S., Huey, R., Hart, W. E., Belew, R. K., and Olson, A. J. 1998. "Automated Docking Using a Lamarckian Genetic Algorithm and an Empirical Binding Free Energy Function." *J. Comput. Chem.* 19: 1639.

S.I. 1. PDOS with Orbital Contribution of *trans*-forms of **1-3**.

trans-form of **1**

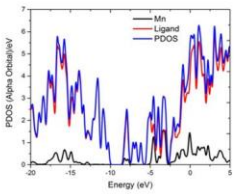

Alpha MOs	Mn	Ligands
L+5	1	99
L+4	2	98
L+3	23	77
L+2	0	100
L+1	6	94
LUMO	28	72
HOMO	1	99
H-1	0	100
H-2	0	100
H-3	1	99
H-4	0	100
H-5	0	100

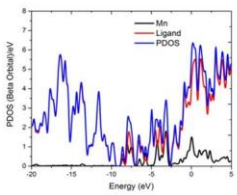

Beta MOs	Mn	Ligand
L+5	19	81
L+4	18	82
L+3	27	73
L+2	92	8
L+1	39	61
LUMO	2	98
HOMO	3	97
H-1	2	98
H-2	0	100
H-3	2	98
H-4	2	98
H-5	0	100

trans-form of **2**

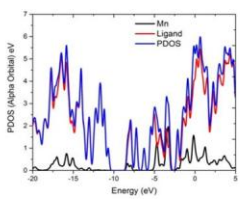

Alpha MOs	Mn	Ligands
L+5	1	99
L+4	1	99
L+3	3	97
L+2	21	79
L+1	1	99
LUMO	31	69
HOMO	1	99
H-1	0	100
H-2	1	99
H-3	0	100
H-4	0	100
H-5	0	100

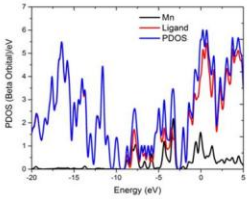

Beta MOs	Mn	Ligands
L+5	22	78
L+4	37	63
L+3	19	81
L+2	90	10
L+1	39	61
LUMO	1	99
HOMO	2	98
H-1	1	99
H-2	0	100
H-3	1	99
H-4	1	99
H-5	0	100

trans-form of **3**

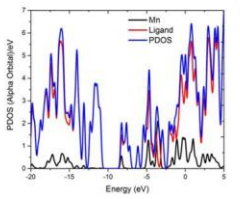

Alpha MOs	Mn	Ligand
L+5	0	100
L+4	0	100
L+3	1	99
L+2	3	97
L+1	0	100
LUMO	56	44
HOMO	1	99
H-1	1	99
H-2	0	100
H-3	0	100
H-4	0	100
H-5	0	100

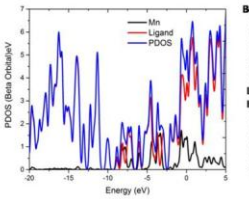

Beta MOs	Mn	Ligand
L+5	86	14
L+4	61	39
L+3	4	96
L+2	100	0
L+1	44	56
LUMO	1	99
HOMO	2	98
H-1	0	100
H-2	1	99
H-3	0	100
H-4	2	98
H-5	0	100

S.I. 2. UV-VIS Spectra and possible transitions in *trans*-forms of **1-3** and Cu(II) analogues

1 and its Cu(II) analogue2

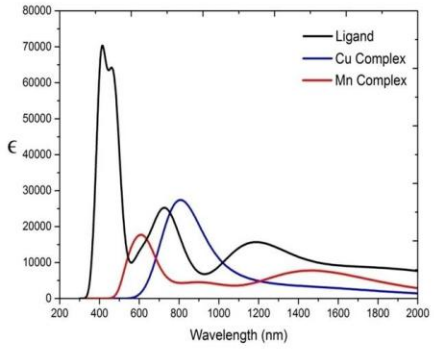

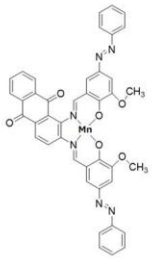

trans-form of **1**

	Wavelength (nm)	Osc Strength	Symmetry	Major Contribution	Minor Contribution
H_2L^1	400.556	0.2	Singlet-A	H-1->L+3 (18%), H-1->L+4 (25%), HOMO->L+5 (24%)	H-17->LUMO (4%), H-12->LUMO (3%), HOMO->L+4 (9%)
	480.038	0.3	Singlet-A	HOMO->L+2 (53%), HOMO->L+4 (10%)	H-16->LUMO (6%), H-15->LUMO (3%), H-13->LUMO (2%), H-12->LUMO (3%), H-7->LUMO (4%), H-4->L+1 (3%)
	734.286	0.2	Singlet-A	H-5->LUMO (14%), HOMO->L+1 (76%)	H-4->LUMO (3%), H-1->LUMO (4%)
	1180.352	0.2	Singlet-A	H-1->LUMO (76%), HOMO->LUMO (21%)	HOMO->L+1 (3%)
Cu(II) analogue of 1	837.109	0.06	2.590-A	H-5(B)->LUMO(B)(12%), H-4(B)->L+1(B) (12%)	H-7(A)->LUMO(A) (5%), H-4(A)->LUMO(A) (4%), H-10(B)->L+1(B) (8%), H-9(B)->LUMO(B) (3%), H-9(B)->L+1(B) (7%), H-8(B)->LUMO(B) (8%), H-8(B)->L+1(B) (3%), H-6(B)->LUMO(B) (8%), H-4(B)->LUMO(B) (7%), H-3(B)->L+1(B) (9%), H-2(B)->L+1(B) (2%)
1	549.429	0.1	6.259-A	H-1(B)->L+4(B) (32%)	H-13(A)->L+2(A) (5%), H-12(A)->L+2(A) (7%), H-9(A)->L+2(A) (4%), H-4(A)->LUMO(A) (2%), H-3(A)->L+2(A) (2%), H-1(A)->L+1(A) (4%), H-1(A)->L+5(A) (3%), H-5(B)->L+1(B) (2%), H-4(B)->L+4(B) (2%), H-1(B)->L+5(B) (2%), H-1(B)->L+7(B) (2%), HOMO(B)->L+4(B) (2%), HOMO(B)->L+6(B) (2%), HOMO(B)->L+7(B) (5%)

Continued.

2 and its Cu(II) analogue

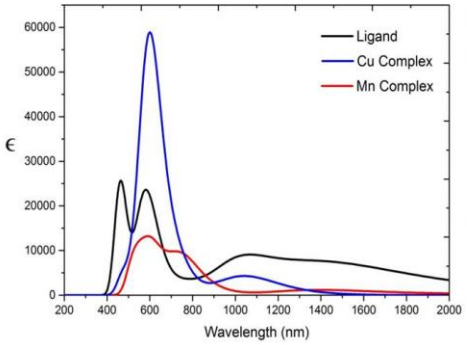

	Wavelength (nm)	Osc Strength	Symmetry	Major Contribution	Minor Contribution
H_2L^2	470.136	0.1	Singlet-A	H-14->LUMO (24%), HOMO->L+5 (45%)	H-16->LUMO (4%), H-4->L+3 (3%), H-1->L+4 (2%)
	581.430	0.2	Singlet-A	HOMO->L+3 (80%)	H-10->LUMO (3%), H-5->L+1 (4%), H-1->L+3 (3%)
	1036.224	0.1	Singlet-A	H-1->L+1 (19%), HOMO->L+1 (78%)	
	607.438	0.5	2.872-A	H-10(A)>LUMO(A)(20%), H-6(A)->LUMO(A)(17%), H-3(A)->LUMO(A)(10%), H-11(B)->LUMO(B)(14%)	H-13(A)->L+1(A) (2%), H-11(A)->LUMO(A)(2%), H-8(A)->LUMO(A) (2%), HOMO(A)->L+1(A) (4%), H-12(B)->L+1(B) (3%), H-9(B)->LUMO(B) (3%), H-5(B)->LUMO(B) (2%), HOMO(B)->L+1(B) (6%)
Cu(II) analogue of 2	525.534	0.09	6.213-A	H-10(A)->L+3(A)(22%), H-3(A)->L+5(A) (10%), HOMO(B)->L+7(B) (10%)	H-12(A)->L+3(A) (4%), H-11(A)->L+3(A) (3%), H-10(A)->L+2(A) (3%), H-9(A)->L+3(A) (2%), H-7(A)->L+3(A) (2%), H-3(A)->L+4(A) (3%), H-2(A)->L+3(A) (3%), H-1(A)->L+5(A) (2%), HOMO(A)->L+5(A) (3%), H-4(B)->L+4(B) (2%), H-3(B)->L+4(B) (3%), HOMO(B)->L+8(B) (9%)
2	739.189	0.07	6.080-A	H-11(B)>LUMO(B)(12%), H-10(B)>LUMO(B)(11%), H-9(B)->LUMO(B)(50%), H-1(B)->L+1(B) (15%)	

Continued.

3 and its Cu(II) analogue

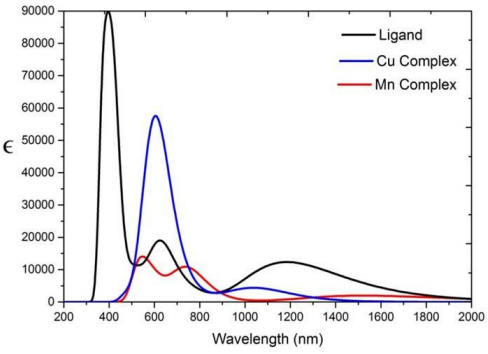

	Wavelength (nm)	Osc Strength	Symmetry	Major Contribution	Minor Contribution
H_2L^3	389.055	0.3	Singlet-A	H-5->L+2 (14%), HOMO->L+5 (53%)	H-4->L+2 (3%), H-1->L+4 (3%), H-1->L+5 (5%), HOMO->L+3 (5%), HOMO->L+4 (4%)
	415.302	0.5	Singlet-A	H-1->L+2 (14%), HOMO->L+3 (40%)	H-16->LUMO (9%), H-15->LUMO (6%), H-14->LUMO (3%), H-2->L+2 (3%), HOMO->L+4 (6%), HOMO->L+5 (3%)
	656.522070491	0.1	Singlet-A	H-4->LUMO (61%), HOMO->L+1 (21%)	H-5->LUMO (4%), H-1->LUMO (2%), HOMO->LUMO (2%)
	595.391	0.4	2.899-A	H-11(A)>LUMO(A)(14%), HOMO(A)->L+1(A)(10%), H-10(B)->LUMO(B)(38%)	H-13(A)->L+1(A) (4%), H-7(A)->LUMO(A) (4%), H-11(B)->LUMO(B)(2%), H-6(B)->LUMO(B) (8%), H-4(B)->L+2(B) (2%), HOMO(B)->L+1(B) (3%)
Cu(II) analogue of 3	535.060	0.07	6.280-A	H-9(A)->L+3(A) (11%), H-8(A)->L+4(A) (10%), H-7(B)->L+1(B) (14%), HOMO(B)->L+6(B) (11%)	H-10(A)->L+1(A) (2%), H-3(A)->L+1(A) (9%), H-3(A)->L+5(A) (3%), H-1(A)->L+1(A) (2%), H-1(A)->L+4(A) (5%), HOMO(A)->L+2(A) (2%), HOMO(A)->L+3(A) (6%), H-11(B)->L+1(B) (2%), H-3(B)->L+3(B) (3%), H-2(B)->L+3(B) (5%)
3	733.287159997	0.1	6.074-A	H-11(B)->LUMO(B) (11%), H-10(B)->LUMO(B) (75%)	H-1(A)->L+4(A) (3%), HOMO(A)->L+3(A) (3%), H-4(B)->L+1(B) (2%), HOMO(B)->L+6(B) (3%)

S.I. 3. UV-VIS Spectra and possible transitions in *trans*-forms of **1-2**

cis-form of **1**

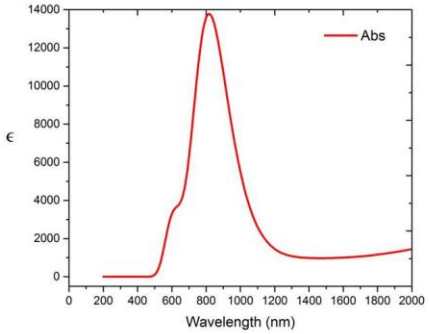

	Wavelength (nm)	Osc Strength	Symmetry	Major Contribution	Minor Contribution
Cis-form of 1	836.262	0.08	6.200-A	HOMO(B)->L+5(B) (36%), HOMO(B)->L+6(B) (22%), HOMO(B)->L+7(B) (11%)	HOMO(A)->L+5(A) (7%), H-7(B)->LUMO(B) (2%), HOMO(B)->L+9(B) (3%), HOMO(B)->L+10(B) (3%)

cis-form of **2**

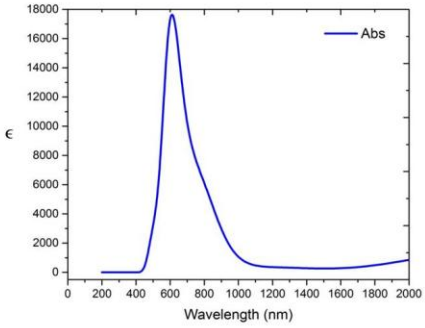

	Wavelength (nm)	Osc Strength	Symmetry	Major Contribution	Minor Contribution
Cis-form of 2	605.598	0.08	6.116-A	H-1(A)->LUMO(A) (12%), HOMO(A)->L+5(A) (23%), HOMO(B)->L+8(B) (18%)	HOMO(A)->L+2(A) (2%), H-11(B)->LUMO(B) (5%), H-10(B)->LUMO(B) (5%), H-9(B)->LUMO(B) (5%), H-6(B)->L+1(B) (3%), H-5(B)->L+1(B) (2%), H-1(B)->L+1(B) (6%)

S.I. 4. PDOS with Orbital Contribution of *cis*-forms of **1-2**.

cis-form of **1**

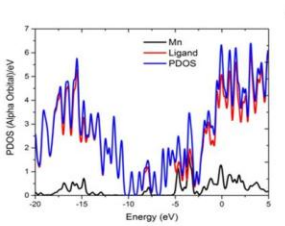

Alpha MOs	Mn	Ligand
L+5	0	100
L+4	2	98
L+3	31	69
L+2	11	89
L+1	16	84
LUMO	0	100
HOMO	0	100
H-1	1	99
H-2	0	100
H-3	0	100
H-4	1	99
H-5	1	99

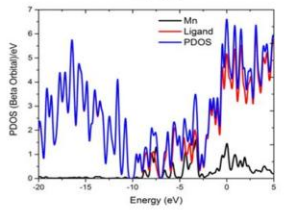

Beta MOs	Mn	Ligand
L+5	13	87
L+4	73	27
L+3	34	66
L+2	7	93
L+1	33	67
LUMO	2	98
HOMO	6	94
H-1	2	98
H-2	2	98
H-3	2	98
H-4	1	99
H-5	0	100

cis-form of **2**

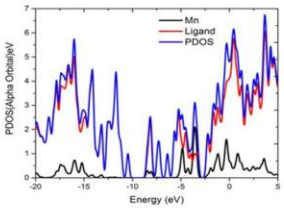

Alpha MOs	Mn	Ligand
L+5	1	99
L+4	1	99
L+3	25	75
L+2	1	99
L+1	1	99
LUMO	29	71
HOMO	0	100
H-1	1	99
H-2	0	100
H-3	0	100
H-4	0	100
H-5	0	100

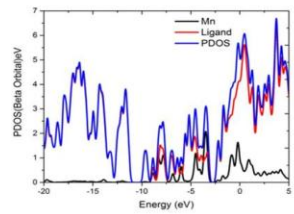

Beta MOs	Mn	Ligand
L+5	23	77
L+4	33	67
L+3	22	78
L+2	84	16
L+1	38	62
LUMO	1	99
HOMO	3	97
H-1	0	100
H-2	0	100
H-3	0	100
H-4	1	99
H-5	0	100

S.I. 5. Details of docking *cis*-form of **1**.

Bond Name	Distance (Å)	Bond category	Bond type
P:POS1:H5 - P:POS1:O4	2.23683	Hydrogen Bond	Carbon Hydrogen Bond
A:LEU399:O - P:POS1	2.63499	Other	Pi-Lone Pair
P:POS1:H24 - A:ALA76:O	2.72308	Hydrogen Bond	Carbon Hydrogen Bond
P:POS1:H23 - A:ASP77:OD1	2.73455	Hydrogen Bond	Carbon Hydrogen Bond
A:ALA403:CA - P:POS1:O3	2.75161	Hydrogen Bond	Carbon Hydrogen Bond
P:POS1:H24 - A:GLN70:OE1	2.75375	Hydrogen Bond	Carbon Hydrogen Bond
A:HIS402:O - P:POS1	2.80636	Other	Pi-Lone Pair
A:ASP77:OD1 - P:POS1	2.85246	Electrostatic	Pi-Anion
A:HIS400:NE2 - P:POS1	2.90308	Other	Pi-Lone Pair
P:POS1:N3 - A:HIS454	2.91289	Other	Pi-Lone Pair
P:POS1:H28 - A:HIS109:O	2.92536	Hydrogen Bond	Carbon Hydrogen Bond
A:ASP424:OD2 - P:POS1	3.12933	Electrostatic	Pi-Anion
A:ASP456:OD2 - P:POS1	3.13155	Electrostatic	Pi-Anion
A:HIS111 - P:POS1	3.40795	Hydrophobic	Pi-Pi Stacked
A:ASP424:OD2 - P:POS1	3.71353	Electrostatic	Pi-Anion
A:HIS400 - P:POS1	3.79501	Hydrophobic	Pi-Pi Stacked
A:HIS454 - P:POS1	4.28387	Hydrophobic	Pi-Pi Stacked
A:GLY67:C,O,PHE68:N - P:POS1	4.32737	Hydrophobic	Amide-Pi Stacked
A:PHE68 - P:POS1	4.38413	Hydrophobic	Pi-Pi Stacked
P:POS1 - A:ALA403	4.58791	Hydrophobic	Pi-Alkyl
A:HIS66 - P:POS1	4.68749	Hydrophobic	Pi-Pi Stacked
A:HIS66 - P:POS1	4.93692	Hydrophobic	Pi-Pi Stacked
P:POS1 - A:LEU459	5.07549	Hydrophobic	Pi-Alkyl

S.I. 6. UV-vis spectra (DMSO) of **1** during photoisomerization

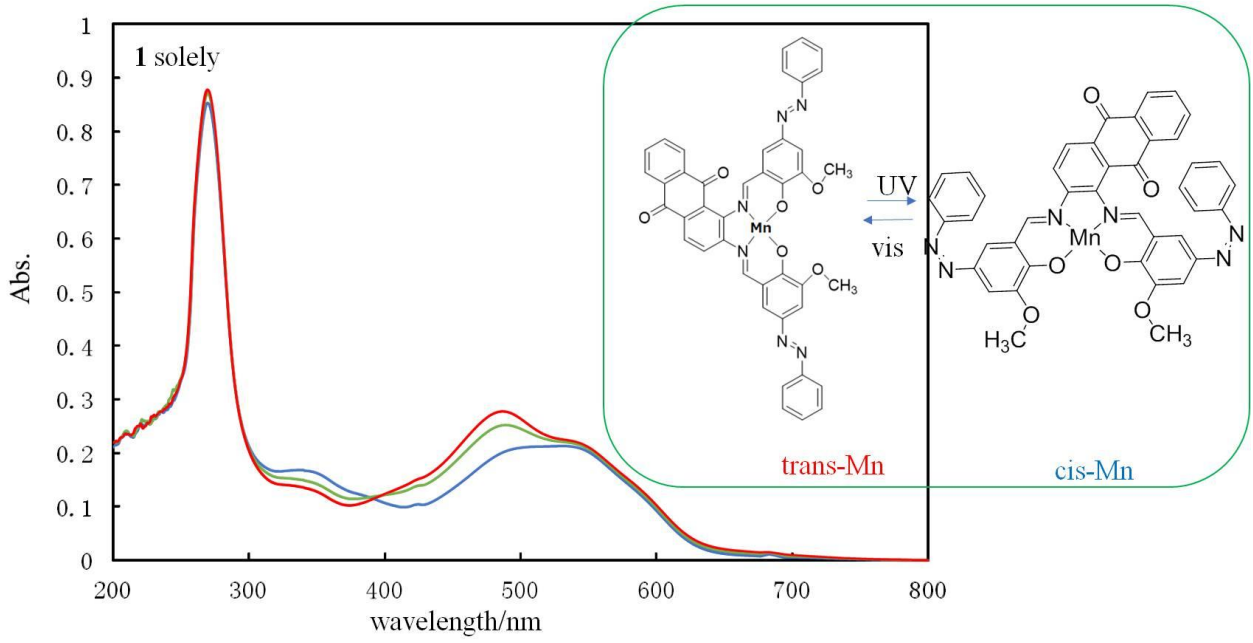

Red: UV 0 min (*trans*-form), Green: UV 5 min, Blue: UV 10 min (*cis*-form)